Engineering oxygen vacancy-rich CeO_x overcoating onto Ni/Al_2O_3 by atomic layer deposition for bi-reforming of methane

Baitang Jin [1], Kaiying Wang [2], Han Yu [1], Xiaoqing He [3,4], and Xinhua Liang [1,2,*]

[1] *Linda and Bipin Doshi Department of Chemical and Biochemical Engineering, Missouri University of Science and Technology, Rolla, Missouri 65409, United States*

[2] *Department of Energy, Environmental and Chemical Engineering, Washington University in St. Louis, St. Louis, Missouri 63130, United States*

[3] *Electron Microscopy Core Facility, University of Missouri, Columbia, Missouri 65211, United States*

[4] *Department of Mechanical and Aerospace Engineering, University of Missouri, Columbia, MO 65211, United States*

* Corresponding author. Email: xinhua.liang@wustl.edu

Abstract

Atomic layer deposition (ALD) was applied to develop CeO_x-overcoated Ni/Al_2O_3 catalyst for bi-reforming of methane (BRM), as the combination of dry reforming of methane (DRM) and steam reforming of methane (SRM). Non-stoichiometric CeO_x thin films were successfully deposited on Ni/Al_2O_3 particles by ALD, which constructed a beneficial Ni-CeO_x interface and modified the catalyst property. Ascribed to the unique ALD growth mode, a high amount of Ce(III) and oxygen vacancies existed in the ALD-deposited CeO_x overcoating. A reduction process before the BRM reaction contributed to the further reduction of Ce(IV) to Ce(III), resulting in more oxygen vacancies. The oxygen vacancies at the Ni-CeO_x interface enabled a high rate of CO_2 activation

and enabled the balance between the activation of CO_2 and H_2O for BRM. Due to its oxygen vacancies as activation sites for CO_2 and H_2O, CeO_x ALD overcoating significantly improved the activity of Ni/Al_2O_3 catalyst and achieved a better control in the H_2/CO ratio with a suitable ratio of $H_2O/CO_2/CH_4$ feed. CeO_x overcoatings enhanced the reducibility of Ni(II) sites and assisted in preventing Ni from oxidation during the BRM reaction. Less carbon deposition was achieved by the Ni/Al_2O_3 catalyst with CeO_x overcoating as ascribed to its better reactant activation capacity.

Keywords: Non-stoichiometric CeO_x; atomic layer deposition (ALD); bi-reforming of methane (BRM); oxygen vacancy

1. Introduction

With the rising greenhouse gas (GHG) emissions, the net-zero target by 2050 set in the Paris Agreement and Conference of the Parties necessitates a technically feasible strategy to chemically recycle captured CO_2 into value-added products for the decarbonization roadmap [1, 2]. Dry reforming of methane (DRM, eq. 1) exhibits remarkable potential in consuming the GHG (i.e., CH_4 and CO_2), utilizing the off-peak energy, and producing syngas (i.e., H_2 and CO) with H_2/CO molar ratio of ~1 as industrial C1-block, whereas the current steam reforming of methane (SRM, eq. 2, with H_2/CO molar ratio of ~3) faces high H_2/CO ratio with the formation of side-product CO_2 [3]. Without reconstructing the present infrastructure, bi-reforming of methane (BRM), which incorporates DRM into SRM, can achieve industrial utilization of CO_2 and production of valuable syngas with desired H_2/CO ratio [1, 3, 4]. Especially, syngas with an H_2/CO molar ratio of ~2 (metgas) can be achieved (eq. 3) by BRM and it is optimal for the production of methanol and dimethyl ether, which are blueprinted as the renewable CO_2-recycling synthetic fuels to substitute

the conventional fossil fuels in the near future [3, 5-7]. Nickel, with low cost and high reactivity for CH_4, has been widely investigated as methane reforming catalysts [1, 8, 9]. However, Ni-based catalysts face the challenge of sintering and coking. Especially, the side reactions (e.g., CH_4 cracking and Boudouard reactions) result in carbon growth and high pressure drop in fixed bed reactors [10-12]. To inhibit carbon growth and accumulation, constructing a metal-oxide interface (e.g., introducing promoter or overcoating) and enhancing the concentration of interfacial oxygen surrounding Ni sites can kinetically accelerate the removal rate of carbon intermediates via CO_2 oxidation [13].

$$CH_4 + CO_2 \rightarrow 2H_2 + 2CO, \qquad \Delta H^0_{298K} = 248\ \mathrm{kJ/mol} \quad (1)$$

$$CH_4 + H_2O \rightarrow 3H_2 + CO, \qquad \Delta H^0_{298K} = 206\ \mathrm{kJ/mol} \quad (2)$$

$$3CH_4 + CO_2 + 2H_2O \rightarrow 8H_2 + 4CO, \qquad \Delta H^0_{298K} = 712\ \mathrm{kJ/mol} \quad (3)$$

CeO_2, with reversible valence states and oxygen vacancies, has been proven to be effective to provide active O sites and enhance the performance of catalysts for methane reforming [14]. The intimate contact between Ni and CeO_2 exhibits a strong influence on the catalytic behavior. For instance, Yan et. al utilized plasma-synthesized Ni/CeO_2-SiO_2 with closer Ni-CeO_2 contact than that of the catalyst prepared by the calcination method for DRM, and achieved better activity and stability due to the more reactive O species at Ni-CeO_2 interface [8]. Besides, the morphology of CeO_2 (e.g., nanorod, nanoparticles, or thin-film) has been reported to play a decisive role on the concentration of oxygen vacancies [15-18], which can participate in CO_2 activation [19]. To develop a highly active and stable catalyst for methane reforming, it is desirable to deposit CeOx with high concentration of oxygen vacancies and construct a sufficient metal-oxide interface.

Atomic layer deposition (ALD) is a gas phase self-limiting thin film coating technology based on cycle-repeatedly sequential surface reactions [20]. With a desired number of ALD cycles, the layer-by-layer growth could be achieved at the atomic level. For heterogeneous catalysts, ALD has been applied to prepare highly dispersed metal clusters as the active catalytic sites, from single atoms to nm-scale nanoparticles (NPs) [20-23]; ALD can also synthesize ultrathin oxide layer or overcoating, which exhibits unique features in generating additional active sites [21, 24], blocking the undesired sites [25], or constructing functional structure [25, 26] for heterogeneous catalysts. Studies showed that the encapsulating structure of ALD oxide film became discontinuous and partially encapsulating on the active metal sites after high-temperature treatment, which effectively exposed the active metal sites and created desirable metal-oxide interfaces [25, 27-29]. Ascribed to the growth mode of ALD, studies showed that the composition of ALD oxide thin film could be non-stochiometric and exhibited unique properties, which differs from the oxides prepared by traditional methods [24, 29, 30]. Considering the importance of interfacial oxygen species, depositing a suitable oxide onto Ni/Al_2O_3 catalyst as overcoating can effectively construct an ideal metal-oxide interface and tune the catalytic performance. In this work, a highly active and coke-resistant CeO_x-Ni/Al_2O_3 catalyst was synthesized by Ni ALD on Al_2O_3 support, followed by CeO_x ALD. CeO_x ALD exhibited unique properties and enhanced the catalytic performance of Ni/Al_2O_3, enabling to tune the H_2/CO ratio for the BRM reaction.

2. Experimental

2.1. Catalyst preparation

92 Ni/Al_2O_3 catalyst was synthesized by depositing Ni NPs onto α-Al_2O_3 NPs (Alfa Aesar, 99+%, 80
93 nm, US3008) using ALD in a home-made fluidized bed reactor [31], as shown in Figure S1.
94 Bis(cyclopentadienyl)nickel ($NiCp_2$, Alfa Aesar) and hydrogen (Airgas, 99.99%) were used as
95 precursors, and N_2 (Airgas, 99.99%) was used as a carrier gas or flush gas. Before ALD, α-Al_2O_3
96 NPs were loaded in the reactor and preheated at 150 ºC overnight to remove moisture. Then, the
97 reactor temperature was set at 300 ºC for Ni ALD. For a typical Ni ALD cycle, $NiCp_2$ was dosed
98 into the ALD reactor by heating a $NiCp_2$ bubbler at 90 ºC and delivering the vaporized $NiCp_2$ with
99 6 mL/min N_2 for 300 s to initiate the first half-reaction. The ALD reactor was flushed by N_2 flush
100 for 600 s to remove excess $NiCp_2$ and by-products, followed by vacuum evacuation for 20 s. For
101 the second half-reaction, 20 mL/min H_2 was dosed into the reactor for 300 s to react with the
102 chemisorbed $NiCp_2$ and generate Ni NPs, followed by the clean-up using N_2 flush and evacuation.
103 In this work, 5 cycles of Ni ALD were applied to synthesize Ni NPs and the catalyst was labeled
104 as Ni/Al_2O_3.
105
106 CeO_x ALD was conducted to deposit CeO_x overcoating onto the Ni/Al_2O_3 catalyst in the same
107 ALD reactor. Tris(i-propylcyclopentadienyl)cerium ($Ce(iPrCp)_3$, Strem Chemicals, 99.9%) and
108 deionized water were used as the precursors for CeO_x ALD and N_2 was used as a carrier gas. The
109 reactor temperature was set at 200 ºC. For a typical CeO_x ALD cycle, $Ce(iPrCp)_3$ was dosed into
110 the reactor by heating a $Ce(iPrCp)_3$ bubbler at 150 ºC and delivering the vaporized $Ce(iPrCp)_3$
111 with 15 mL/min N_2 for 60 s, followed by the reactor clean-up using N_2 flush and evacuation. Then,
112 H_2O was dosed into the reactor for 60 s to react with the chemisorbed $Ce(iPrCp)_3$ and generate the
113 CeO_x overcoating, followed by inert gas flush and vacuum evacuation process. In this work, 10,
114 30, 60, and 90 cycles of CeO_x ALD were applied on the Ni/Al_2O_3 catalyst, and the catalyst was

labeled as 10CeO_x-Ni/Al_2O_3, 30CeO_x-Ni/Al_2O_3, 60CeO_x-Ni/Al_2O_3, and 90CeO_x-Ni/Al_2O_3, respectively. For ease of characterization, 200 cycles of CeO_x ALD were applied on Ni/Al_2O_3 and the catalyst was labeled as CeO_x-Ni/Al_2O_3.

For comparison, Al_2O_3 ALD was conducted to deposit Al_2O_3 overcoating onto the Ni/Al_2O_3 catalyst in the same reactor. Trimethylaluminum (TMA, Sigma-Aldrich) and deionized water were used as the precursors for Al_2O_3 ALD and N_2 was used as the carrier gas. The ALD reaction temperature was 150 ºC for Al_2O_3 ALD. For a typical Al_2O_3 ALD cycle, TMA was dosed into the reactor for 300 s, followed by the reactor clean-up using N_2 flush and evacuation. Then, H_2O was dosed into the reactor for 300 s to react with the chemisorbed TMA and generate Al_2O_3 thin film, followed by the reactor clean-up process. 10 cycles of Al_2O_3 were applied to achieve the similar thickness of CeO_x thin film on 60CeO_x-Ni/Al_2O_3 based the ALD thin film growth rates. The catalyst was labeled as Al_2O_3-Ni/Al_2O_3.

For comparison, liquid-based incipient wetness method was conducted to deposit CeO_2 as a promoter onto the Ni/Al_2O_3 catalyst. Ni/Al_2O_3 particles were impregnated in an aqueous solution of $Ce(NO_3)_3$ (Alfa Aesar, 99.99%) for 1 h (with a similar amount of CeO_x on 60CeO_x-Ni/Al_2O_3), dried at 100 ℃ in an oven, and then calcinated in the air in a tubular furnace at 500 ºC for 3 h. The catalyst was labeled as iwCeO_2/Ni/Al_2O_3.

2.2. Bi-reforming of methane reaction

A home-made fixed bed reactor system was built for bi-reforming of methane reaction, as shown in Figure S2. The reactant control and delivery system were achieved by mass flow controllers

(MKS Instruments) for controlling gas flow rates and a syringe pump (Chemyx Fusion 101) for controlling water flow rate. To ensure the gasification of water, heating tapes (Omega Engineering) were used to heat up the water feeding line to 120 ºC. A quartz tube with an inner diameter of 10 mm was used as a reactor, which was placed vertically and heated by a tubular furnace (Carbolite Gero, Ltd.). A K-type thermocouple (Omega Engineering) was positioned right above the catalyst bed to monitor the reactor temperature. One on-line gas chromatograph (SRI 8610C) was used to analyze the products, with a 6-foot Hayesep D column and TCD detector. A cold trap tank was used to condense any by-product water from the product gas before it entered into the GC.

For the BRM reaction, ~50 mg catalyst particles were loaded on ~30 mg quartz wool in the quartz tube reactor. A reduction procedure was conducted at 800 ºC for 1 h using 20%H_2/80%Ar (v/v%) mixture with a flow rate of 100 mL/min. After reduction, the temperature was set at a desired temperature and the reactant gases (i.e., CH_4, CO_2, and gas-phase H_2O) were introduced into the reactor.

2.3. Catalyst characterizations

Transmission electron microscopy (TEM) was conducted using an FEI Tecnai F20 TEM instrument to measure the Ni particle size and acquire the morphology of the catalysts. X-ray photoelectron spectroscopy (XPS) was conducted using a Kratos Axis 165 X-ray photoelectron spectrometer to determine the chemical states of different elements. XRD was conducted on an X-Pert Multi-purpose diffractometer to access the phase information of the catalysts.

160 H_2-temperature programmed reduction (H_2-TPR) was conducted using a Micromeritics AutoChem
161 II 2920 instrument. The catalysts were first pretreated in Ar at 300 ºC for 1 h. Then, H_2-TPR was
162 performed using 10%H_2/90%Ar (v/v%) from 50 to 900 °C with a temperature increasing rate of
163 10 °C/min. The H_2 pulse chemisorption experiment was also conducted on this Micromeritics
164 AutoChem II 2920 instrument. The sample was first pretreated in a H_2/Ar (mixed at 10/90 vol%)
165 flow for 1 h and flushed in Ar for 1 h at 700 °C. After cooling down to 50 °C in Ar, the samples
166 underwent the cycles of H_2/Ar pulse and Ar pulse.
167
168 Thermogravimetric analysis (TGA) was conducted using a TA Instrument Q50 analyzer. The
169 sample underwent a temperature ramping from room temperature to 200 °C, holding at 200 °C for
170 1 h, and temperature ramping from 200 to 800 °C at 10 °C /min in 40 mL/min Ar.
171
172 CO_2-temperature programmed desorption (CO_2-TPD) and O_2-temperature programmed oxidation
173 (O_2-TPO) were conducted using the methane reforming reactor. A mass spectrometer (Stanford
174 Research System, QMS 200) with a pressure-time mode was used to detect and record the gas
175 signal. The m/e value of the MS signal was taken to identify the gas species (e.g., 40 for Ar, 28 for
176 CO, 44 for CO_2, and 32 for O_2). For CO_2-TPD, the catalyst was first reduced at 800 ºC using H_2,
177 then CO_2 saturation in 20 mL/min 20%CO_2/80%Ar (v/v%) mixture for 1 h at 80 ºC and Ar flush
178 in 20 mL/min Ar for 1 h at 80 ºC. After this pretreatment, CO_2-TPO was performed in Ar, starting
179 from 80 to 700 ºC with a temperature increasing rate of 10 C/min. For O_2-TPO, the spent catalysts
180 were first pretreated in Ar at 100 ºC for 1 h r and then oxidized in 20%O_2/80%Ar (v/v%) from 100
181 to 800 °C.
182

3. Results and Discussion

3.1. Material characterizations

TEM was conducted to determine the morphology of the Ni/Al_2O_3 and $60CeO_x$-Ni/Al_2O_3 catalysts. As shown in Figure 1a, the average size of Ni NPs (in oxidized state) on the ALD-prepared Ni/Al_2O_3 was 2.7 ± 0.9 nm, which is much smaller than those prepared by the traditional incipient wetness method. After 60 cycles of CeO_x ALD, the average size of Ni NPs (in oxidized state) on $60CeO_x$-Ni/Al_2O_3 was about 2.9 ± 1.0 nm, which was almost the same as that of the pristine Ni/Al_2O_3. Since the CeO_x ALD process was conducted at a mild temperature of 200 ºC, there was no obvious sintering of Ni NPs during the CeO_2 ALD coating process. For the reduced catalysts, the average size of the reduced Ni/Al_2O_3 catalyst is 9.7 ± 2.3 nm and the average size of the reduced $60CeO_x$-Ni/Al_2O_3 catalyst is 6.2 ± 1.5 nm, which indicates the CeO_x overcoating inhibited the sintering of the Ni during the high-temperature reduction process. As a bottom-up synthesis strategy, ALD can create an ultra-thin CeO_x overcoating on Ni/Al_2O_3 surface conformally and help prevent sintering. The lattice spacing of 0.203 nm could be observed with the HRTEM analysis, which was ascribed to the (111) of metallic Ni. The element mapping result in Figure 1f exhibited the uniform distribution of CeO_x overcoating on both Ni and Al_2O_3, which confirms the Ni-CeO_x interface. In addition, XRD was conducted to determine the phase structure of Ni/Al_2O_3 and CeO_x-Ni/Al_2O_3, as shown in Figure S3. It could be seen that the main peaks were assigned to α-Al_2O_3, with a small amount of NiO. The peaks assigned to any cerium oxide could be hardly seen, probably due to the low loading or the amorphous structure.

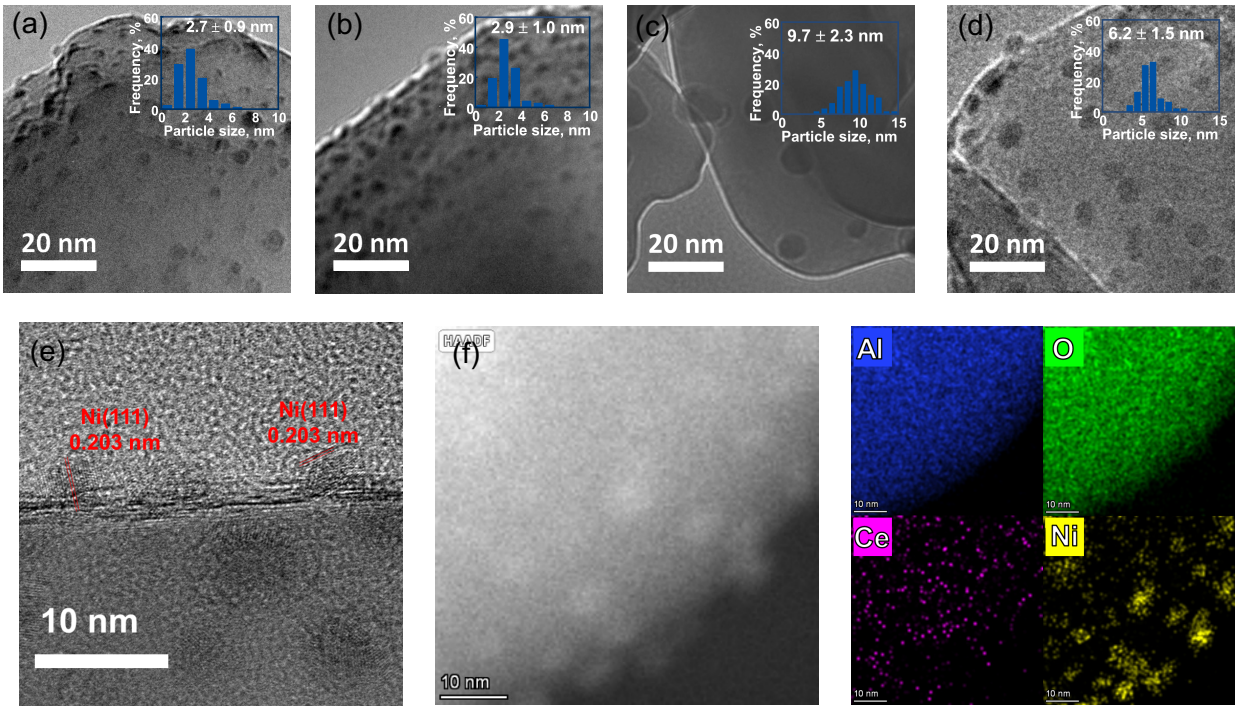

Figure 1. TEM images of (a) fresh Ni/Al_2O_3, (b) fresh $60CeO_x$-Ni/Al_2O_3, (c) reduced Ni/Al_2O_3, and (d-f) reduced $60CeO_x$-Ni/Al_2O_3. (f) EDS elemental mapping of Al, O, Ce, and Ni for reduced $60CeO_x$-Ni/Al_2O_3. The inset images show the size distribution of Ni NPs.

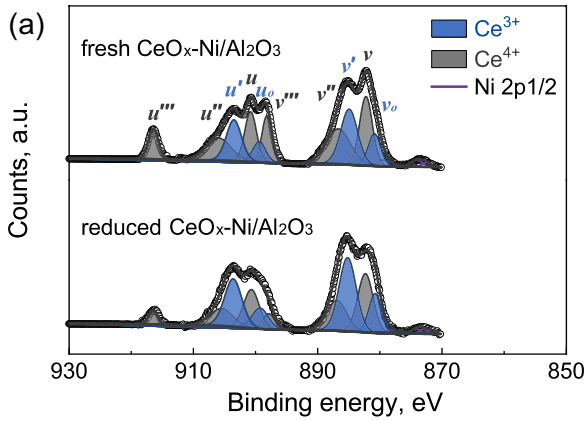

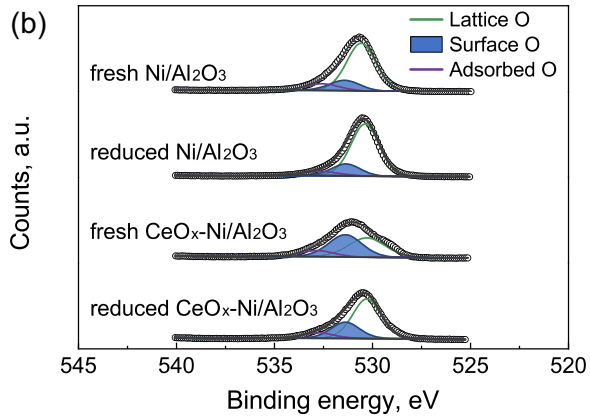

211

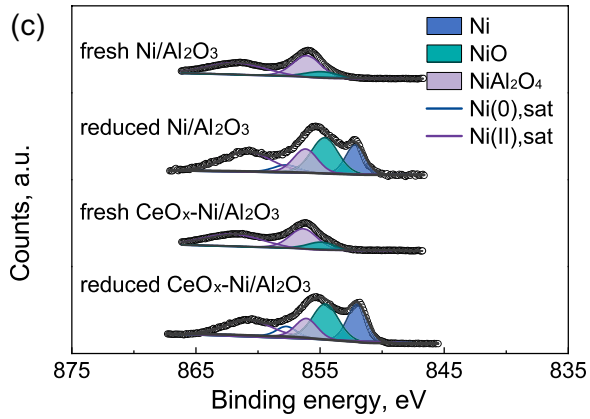

212

213 Figure 2. XPS spectra of (a) Ce3d for fresh CeO_x-Ni/Al_2O_3 and reduced CeO_x-Ni/Al_2O_3, (b) O 1s,
214 and (c) Ni 2p3/2 for fresh Ni/Al_2O_3, reduced Ni/Al_2O_3, fresh CeO_x-Ni/Al_2O_3, and reduced CeO_x-
215 Ni/Al_2O_3.

216

217 To examine the property of CeO_x thin films prepared by ALD, XPS was conducted on the fresh
218 and reduced ALD-prepared CeO_x-Ni/Al_2O_3 and iwCeO_2/Ni/Al_2O_3 catalysts in Figure 2 and Figure
219 S4. All spectra were calibrated by fixing adventitious carbon at 284.5 eV (C1s in Figure S4). For
220 the Ce element in Figure 2a, the Ce(IV) peaks included v at 882.3 eV, v'' at 886.7 eV, v''' at 897.8
221 eV, u at 899.3 eV, u'' at 903.5 eV, and u''' at 916.4 eV [32, 33]. The Ce(III) peaks included v_o at
222 880.8 eV, v' at 885.2 eV, u_o at 899.3 eV and u' at 903.5 eV [32, 33]. To have a quantitative

comparison, the Ce(III) contents were calculated from the ($v_o + v' + u_o + u'$)% for the ALD-prepared and IW-prepared catalysts. Besides, the characteristic u''' peak, without any overlapping with other peaks, could represent the relative Ce(IV) content and was used to indicate the Ce(IV) amount. The Ce(III) content of the fresh ALD-prepared CeO_x-Ni/Al_2O_3 was 38.0%, with u''' peak as Ce(IV) representative at 4.7%. Based on the Ce 3d results, there was more Ce(III) in the ALD-prepared CeO_x-Ni/Al_2O_3 catalyst. For cerium oxide, the content of Ce(III) is generally considered a significant indicator of the oxygen storage capacity, which assists the surface reaction and enhances the catalytic activity [33]. For the ALD-prepared catalyst, the higher amount of Ce(III) should be ascribed to the unique ALD growth mode, because Ce(iPrCp)$_3$ and H_2O would react to form Ce(OH)$_3$ initially, and the ultra-thin film structure could favor the existence of Ce(III) [34-36]. Therefore, the ALD-prepared CeO_x overcoating had more Ce(III) than that prepared by the traditional liquid method and could participate in the surface reaction during methane reforming. During the H_2-reduction process, the chemical states of Ce in Figure 2a and O in Figure 2b also significantly changed. In the spectrum of Ce 3d, there was a higher Ce(III) content for CeO_x-Ni/Al_2O_3, with the Ce(III) ratio of 50.8% based on ($v_o + v' + u_o + u'$)% and the diagnostic peak (u''') of 1.9 % for Ce(IV). For the IW-prepared iwCeO_2/Ni/Al_2O_3 catalyst, the fresh catalyst had a Ce(III) content at 22.4% and u'''% peak as Ce(IV) representative at 6.4%. After reduction, the reduced catalyst had a Ce(III)% content of 42.7 % and u'''% of 4.6 % for the iwCeO_2/Ni/Al_2O_3 catalyst. Compared with the spectra of the fresh CeO_x-Ni/Al_2O_3 catalysts with Ce(III)% of 40.0 % and u'''% of 4.8 %, the Ce(III) content for the reduced catalyst was higher, indicating the reduction of Ce(IV). Owning to the variable valences of Ce(III) and Ce(IV), Ce(IV) was reduced to Ce(III) during H_2-reduction, and more oxygen vacancies were generated to keep the electronic balance of Ce(III) [18, 41].

The oxygen species were investigated using XPS for Ni/Al_2O_3, ALD-overcoated CeO_x-Ni/Al_2O_3, ALD-overcoated Al_2O_3-Ni/Al_2O_3, and IW-promoted $iwCeO_2/Ni/Al_2O_3$. The O species were deconvoluted to three peaks, including the lattice O at ~ 530.5 eV for O of the metal oxide, the surface O at ~ 531.5 eV for low coordinated oxygen atoms, and the adsorbed O at ~532.7 eV from adsorbed H_2O [37]. Especially, the surface oxygen consists of hydroxyl oxygen and deficient oxygen sites, which are important surface species. As shown in Figure 2b, the content of surface O in Ni/Al_2O_3 was about ~15%, which was smaller than ~45% of the CeO_x-Ni/Al_2O_3 catalyst. For comparison, the content of surface O for the ALD-overcoated Al_2O_3-Ni/Al_2O_3 catalyst reached ~54% and the content of surface O for IW-promoted $iwCeO_2/Ni/Al_2O_3$ reached ~23% in Figure S4. For the ALD-overcoated catalysts, the high content of the surface O indicated a large number of hydroxyls, regardless of CeO_x ALD or Al_2O_3 ALD overcoating. Besides, the higher content of surface O in the $iwCeO_2/Ni/Al_2O_3$ catalyst indicated that the CeO_2 promoter also increased the surface O for Ni/Al_2O_3 and didn't decrease after high temperature reduction, which was ascribed to the oxygen vacancies with Ce^{4+}/Ce^{3+}. Therefore, the surface O of the ALD-overcoated CeO_x-Ni/Al_2O_3 resulted from both the hydroxyl groups and oxygen vacancies. For O 1s of the samples after reduction, the surface O for ALD-overcoated CeO_x-Ni/Al_2O_3 was about 26.4 %, which was higher than 17.2% for Ni/Al_2O_3, 20.1% for Al_2O_3-Ni/Al_2O_3, and 21.0% for $iwCeO_2/Ni/Al_2O_3$. For the ALD-overcoating catalysts (i.e., CeO_x-Ni/Al_2O_3 and Al_2O_3-Ni/Al_2O_3), the surface O significantly decreased after high-temperature reduction, which was ascribed to the removal of hydroxyl groups at high temperature, whereas the CeO_x-Ni/Al_2O_3 catalyst still had a high amount of surface oxygen. Comparing CeO_x-Ni/Al_2O_3 and Al_2O_3-Ni/Al_2O_3, the higher surface O of CeO_x-Ni/Al_2O_3 should result from the oxygen vacancies. The higher amount of oxygen vacancies after

reduction for reduced CeO_x-Ni/Al_2O_3 was also confirmed by the spectra of Ce 3d. For the bi-reforming of methane, the high amount of oxygen vacancies could serve as the activation sites for CO_2 and enhance the catalytic performance.

Figure 2 and Figure S4 depict the XPS spectra for the reduced Ni/Al_2O_3, reduced CeO_x-Ni/Al_2O_3, reduced Al_2O_3-Ni/Al_2O_3, and reduced iwCeO_2/Ni/Al_2O_3 catalysts. For Ni 2p 3/2, the peaks could be deconvoluted into different Ni species as metallic Ni at ~ 852.1eV, NiO at ~854.5 eV, $NiAl_2O_4$ at ~856.2 eV, and satellite peaks due to shake-up phenomena, including Ni(0),sat at ~857.8 eV and Ni(II),sat at ~ 860.8 eV [38, 39]. Especially, the spinel $NiAl_2O_4$ was highly thermal stable with a reduction temperature of ~800 ºC, whereas NiO was easily reduced to Ni at high temperatures and highly reductive DRM reaction conditions. For the fresh catalyst (Figure S4), a high amount of $NiAl_2O_4$ indicates that the interaction between NiO and Al_2O_3 for ALD-prepared Ni/Al_2O_3 was very strong, which was due to the chemisorption-based growth mechanism [40]. Under this circumstance, the presence of $NiAl_2O_4$ after reduction treatment could be considered an incomplete reduction, which could lead to the activity loss. Comparing the different catalysts after reduction in Figure 2c and Figure S4e, the content of $NiAl_2O_4$ was 17.6% for Ni/Al_2O_3, 13.8% for CeO_x-Ni/Al_2O_3, 26.4% for Al_2O_3-Ni/Al_2O_3, and 14.1% for iwCeO_2/Ni/Al_2O_3. Based on the chemical states of Ni, the CeO_x ALD overcoating, or CeO_2 IW promoter significantly enhanced the reducibility, whereas the Al_2O_3 ALD overcoating exhibited a negative effect on the reducibility due to the formation of $NiAl_2O_4$. In this case, CeO_x ALD effectively weakened the metal-support interaction (i.e., Ni-Al_2O_3 interaction) and released more Ni from $NiAl_2O_4$, while Al_2O_3 ALD overcoating resulted in the formation of more $NiAl_2O_4$.

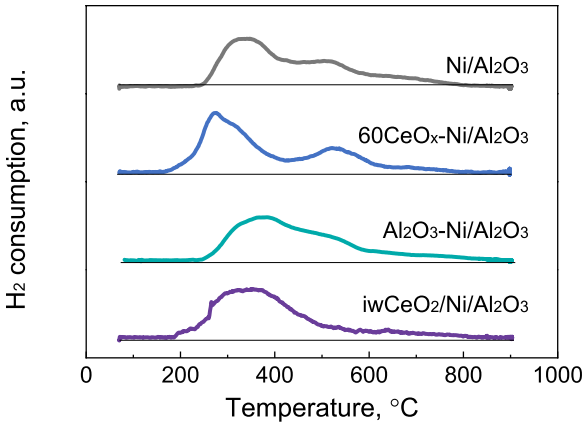

291

292 Figure 3. H_2-TPR spectra of Ni/Al_2O_3, $60CeO_x$-Ni/Al_2O_3, Al_2O_3-Ni/Al_2O_3, and $iwCeO_2/Ni/Al_2O_3$.

293

294 To characterize the metal-support interactions and probe the effects of CeO_x ALD thin film, H_2-
295 TPR was conducted for Ni/Al_2O_3, ALD-overcoated $60CeO_x$-Ni/Al_2O_3, ALD-overcoated Al_2O_3-
296 Ni/Al_2O_3, and IW-promoted $iwCeO_2/Ni/Al_2O_3$, as shown in Figure 3. Depending on the extent of
297 Ni diffusion into the Al_2O_3 lattice, a higher reduction temperature is necessary for the species with
298 a greater extent of diffusion/interaction and various species can be identified by TPR [42],
299 including free NiO without any interaction, NiO-Al_2O_3 with interaction, and $NiAl_2O_4$ with spinel
300 crystallization [40, 42]. For Ni/Al_2O_3, the dominant peak at ~340 ºC was assigned to NiO, the peak
301 at ~515 ºC was assigned to NiO-Al_2O_3, and the peak >700 ºC was assigned to $NiAl_2O_4$. Therefore,
302 Ni(II) peaks in Ni/Al_2O_3 mainly consisted of free NiO and NiO-Al_2O_3, with a reduction degree at
303 72%. For ALD-overcoated $60CeO_x$-Ni/Al_2O_3, the NiO peak was at ~280 ºC and the NiO-Al_2O_3
304 peak was at ~520 ºC. Clearly, CeO_x ALD facilitated the reduction process of the free NiO sites
305 because the free NiO shifted to a lower temperature. The reduction degree for the $60CeO_x$-
306 Ni/Al_2O_3 was about 77%, indicating that the CeO_x ALD promoted the reduction of Ni sites. For
307 ALD-overcoated Al_2O_3-Ni/Al_2O_3, the NiO peak and the NiO-Al_2O_3 peak almost remained in the

same position as those of Ni/Al_2O_3 with similar reduction degree at 71%, but the peaks became broadened, especially the $NiO\text{-}Al_2O_3$ peak, indicating that Al_2O_3 ALD films interacted with Ni sites. Regarding the reducibility, CeO_x ALD overcoating was beneficial to the catalytic activity as compared to Al_2O_3 as the overcoating material. As for $iwCeO_2/Ni/Al_2O_3$, the overall peak was shifted to lower temperatures, including ~320 ºC for NiO and ~470 ºC for $NiO\text{-}Al_2O_3$, with a reduction degree of 79%. Especially, the promoting effect of IW CeO_2 on $NiO\text{-}Al_2O_3$ might arise from the interaction between $NiO\text{-}CeO_2$ and the possible formation of $NiO\text{-}CeO_2$ after calcination, because the introduction of CeO_2 by the incipient wetness method requires a high temperature calcination at 500 ºC. The difference between ALD-overcoated $CeO_x\text{-}Ni/Al_2O_3$ and IW-promoted $iwCeO_2/Ni/Al_2O_3$ could result from the morphology of ALD CeO_x films, because the role of CeO_x overcoating was prepared by surface modification instead of bulk transformation. Therefore, CeO_x ALD provided an efficient $Ni\text{-}CeO_x$ interface and promoted the reducibility of Ni sites for the Ni/Al_2O_3 catalyst.

Although the stoichiometry of the bi-reforming of methane can be realized by the combination of SRM and DRM, the competition between SRM and DRM reactions should be considered for practical application. Especially, the surface reaction competition between SRM and DRM can be determined by the activation process of H_2O and CO_2 on the surface oxygen sites. To evaluate the surface oxygen and the CO_2 affinity, CO_2 temperature-program desorption (CO_2-TPD) was performed. According to the desorption temperature, the basic sites can be classified as weak basic sites < 200 ºC for physical adsorption or Brønsted basic sites (e.g., -OH group), medium basic sites at 200-350 ºC for Lewis acid-base pair $Ce^{4+}\text{-}O^{2-}$, and strong basic sites >350 ºC for oxygen vacancies or oxygen defects [33, 43]. As shown in Figure 4, the peaks for the Ni/Al_2O_3 catalyst

mainly consisted of weak basic sites due to the acidic and -OH-rich properties of Al_2O_3. For the same reason, Al_2O_3 ALD failed to enhance the medium basic sites or strong basic sites of the catalyst. In contrast, the addition of CeO_2 enhanced both the basic sites and strong basic sites by IW or ALD method, because of the basic nature of CeO_2. However, the ALD-deposited CeO_x exhibited stronger basic properties in terms of quantity and strength, and thus a higher CO_2 affinity than that of the IW-prepared CeO_2. For $iwCeO_2/Ni/Al_2O_3$, the introduction of CeO_2 by the IW method significantly increased the medium basic sites and provided a small amount of the strong basic sites. For $60CeO_x$-Ni/Al_2O_3, the deposition of CeO_x by ALD brought both medium basic sites and strong basic sites, especially for the strong basic sites. In comparison, the high amount of strong basic sites indicated there were more oxygen vacancies for the catalyst with CeO_x ALD overcoating. The high CO_2 affinities and special oxygen sites for CeO_x ALD overcoated catalyst should result from the thin-film structure and unique growth mode. It has been reported that the oxygen vacancies of CeO_2 can be tuned by its morphology and structure and a thin film structure enabled the high amount of oxygen vacancies [15-18]. As ascribed to the layer growth mode of ALD thin films [36], the Ni/Al_2O_3 catalyst with CeO_x ALD overcoating would have enhanced catalytic activity due to the oxygen vacancies of CeO_x.

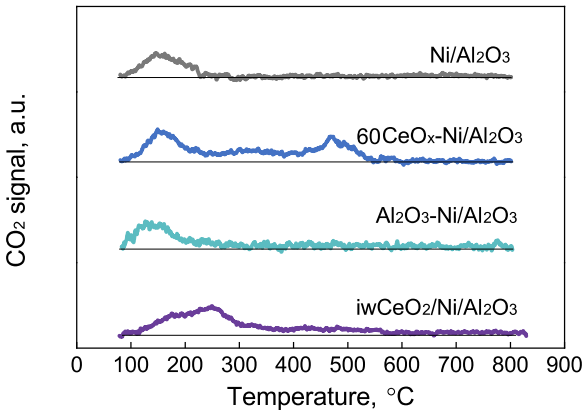

Figure 4. CO_2-TPD spectra of Ni/Al_2O_3, $60CeO_x$-Ni/Al_2O_3, Al_2O_3-Ni/Al_2O_3, and $iwCeO_2/Ni/Al_2O_3$.

3.2. Catalytic performance for bi-reforming of methane

The equilibrium of bi-reforming of methane by co-feeding CH_4, H_2O, and CO_2 was calculated using the Gibbs reactor and Soave-Redlich-Kwong equation of state in ChemCAD, as shown in Figure S5. At varying temperatures, the equilibrium conversion of CH_4 was almost the same at all conditions, but the H_2/CO ratio was very different and varied with the feeding. Here, the H_2/CO ratio from the direct stoichiometric combination of SRM and DRM was used for the comparison with the equilibrium value (see Supporting Information). The difference between the direct stoichiometric value and the equilibrium value was mainly caused by the water-gas shift reaction or reverse water-gas shift reaction (WGS/RWGS). A higher temperature drives the equilibrium H_2/CO molar ratio towards 2, indicating a weaker effect of the WGS/RWGS at a higher temperature. Besides, the H_2/CO ratio exhibited a tunable ratio at varying inlet feed of CH_4, H_2O, and CO_2.

Bi-reforming of methane with $CH_4/H_2O/CO_2$=3/2/1 as a feedstock was conducted using the Ni/Al_2O_3 and ALD CeO_x-overcoated Ni/Al_2O_3 catalysts. Figures 5a and 5b show the CH_4 conversion and H_2/CO for BRM reaction at 850 ºC. As shown in Figure 5a, the CH_4 conversion of Ni/Al_2O_3 reached 61.9% at the initial stage, and then gradually decreased to 56.4% after 72 h at 850 ºC. In contrast, the CeO_x-overcoated Ni/Al_2O_3 catalyst exhibited better stability and activity. Notably, all CeO_x-overcoated Ni/Al_2O_3 catalysts exhibited an activation process in the initial 5 h of reaction, which might be ascribed to the formation of $CeAlO_3$ and further reduction of $NiAl_2O_4$

to metallic Ni, as discussed in our previous work [40, 44], and then a stable conversion could be reached. In this work, 60 cycles of CeO_x exhibited an optimal effect on the Ni/Al_2O_3 catalyst for the BRM reaction. The highest conversion at 87.2% was achieved for the $60CeO_x$-Ni/Al_2O_3 catalyst due to the optimum loading of the CeO_2 overcoating with 60 cycles of CeO_2 ALD, which is much better than that of the uncoated, $10CeO_x$-Ni/Al_2O_3, $30CeO_x$-Ni/Al_2O_3, and $90CeO_2$-Ni/Al_2O_3 catalysts. In Figure 5b, the H_2/CO of Ni/Al_2O_3 and CeO_x-overcoated Ni/Al_2O_3 reached ~2.05, which is close to the value of 2 for the stoichiometric combination DRM/SMR with a feedstock ratio of $CH_4/H_2O/CO_2$=3/2/1.

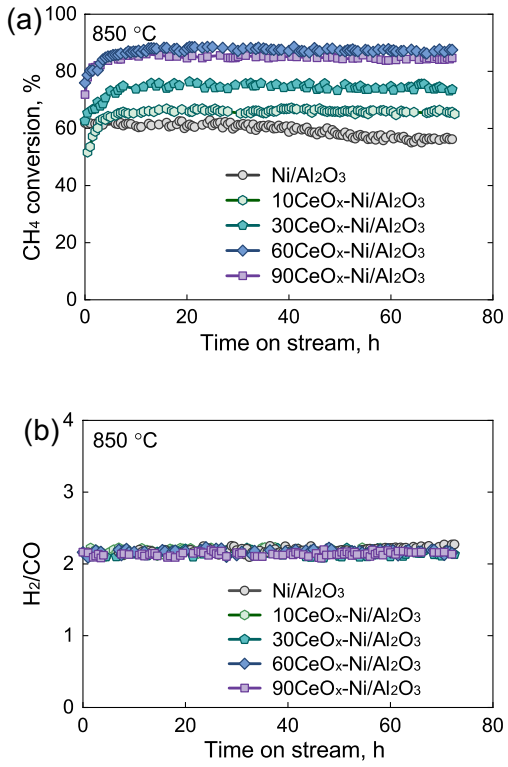

Figure 5. (a) CH_4 conversion and (b) H_2/CO ratio of BRM as a function of time on stream using Ni/Al_2O_3, $10CeO_x$-Ni/Al_2O_3, $30CeO_x$-Ni/Al_2O_3, $60CeO_x$-Ni/Al_2O_3, and $90CeO_x$-Ni/Al_2O_3. Reaction conditions: 50 mg catalyst, 30 mL/min CH_4, 10 mL/min CO_2, 20 mL/min H_2O (gas phase), at 850 °C.

Bi-reforming of methane with $H_2O/CO_2/CH_4/=2/1/3$ was also tested at 750 ºC, as shown in Figure 6. The deactivation of Ni/Al_2O_3 at 750 ºC was more severe than the test at 850 ºC using the same catalyst. The CH_4 conversion for Ni/Al_2O_3 decreased from 39.4% to 19.8% in 72 h, which could be ascribed to the oxidation of the Ni surface and coke formation at a lower reaction temperature. The Al_2O_3 ALD overcoated Al_2O_3-Ni/Al_2O_3 catalyst and the CeO_2 IW promoted $iwCeO_2/Ni/Al_2O_3$ catalyst exhibited better stability than that of Ni/Al_2O_3, but there was still gradual deactivation. In contrast, the CeO_x ALD overcoated $60CeO_x$-Ni/Al_2O_3 catalyst greatly enhanced the stability and activity for BRM, with a stable conversion at 53.5% during a test of 150 h. As for the product, the H_2/CO ratio of BRM using the Ni/Al_2O_3 catalyst increased from 2.45 to 2.88, which could be ascribed to the limited water-gas shift reaction. For the $60CeO_x$-Ni/Al_2O_3 catalyst, the H_2/CO ratio was kept at ~2.34. Therefore, the CeO_x ALD overcoating successfully decorated the Ni sites and enhanced the catalytic performance due to its high oxygen vacancy properties and sufficient Ni-CeO_x interface.

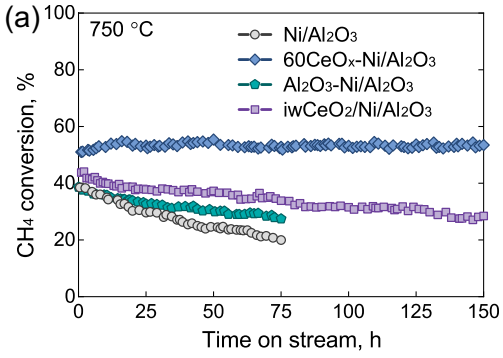

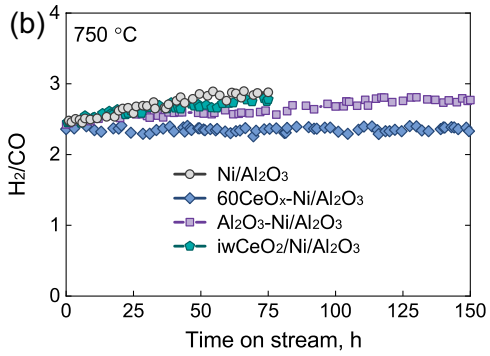

Figure 6. (a) CH_4 conversion and (b) H_2/CO ratio of BRM as a function of time on stream using Ni/Al_2O_3, $60CeO_x$-Ni/Al_2O_3, Al_2O_3-Ni/Al_2O_3, and $iwCeO_2/Ni/Al_2O_3$ as catalysts. Reaction conditions: 50 mg catalyst, 30 mL/min CH_4, 10 mL/min CO_2, and 20 mL/min H_2O (gas phase), and 750 °C.

The catalytic behavior of uncoated Ni/Al_2O_3 and $60CeO_x$-Ni/Al_2O_3 for methane reforming was systematically tested at different temperatures. Figure 7 depicts the CH_4 conversion and H_2/CO molar ratio for BRM with an inlet feed of $H_2O/CO_2/CH_4$=2/1/3 at different temperatures. In Figure 7a, the enhanced activity was observed for $60CeO_2$-Ni/Al_2O_3 at varying temperatures, verifying the promoting effects of CeO_x ALD overcoating. In Figure 7b, the H_2/CO ratio for uncoated Ni/Al_2O_3 and $60CeO_x$-Ni/Al_2O_3 was higher than the value based on the stoichiometric combination (i.e., H_2/CO=2) or the equilibrium ratio, especially at low temperatures. On one hand, the deviation between the practical H_2/CO ratio of BRM products and the equilibrium H_2/CO ratio might be explained by the severe water gas shift reaction. On the other hand, BRM is based on the catalytic dissociation of CH_4 on Ni sites and the following oxidation by H_2O or CO_2, so the H_2/CO ratio in the products should be directly related to the activation process of H_2O or CO_2. Therefore, the difference of H_2/CO ratio for the reaction catalyzed by Ni/Al_2O_3 and $60CeO_2$-Ni/Al_2O_3 indicated

418 that CeO_x overcoating could affect the reactant activation. Therefore, the lower H_2/CO ratio for
419 $60CeO_x$-Ni/Al_2O_3 indicated that the CeO_x overcoating could have a better capability in CO_2
420 activation, which was ascribed to the oxygen vacancies of CeO_x ALD.

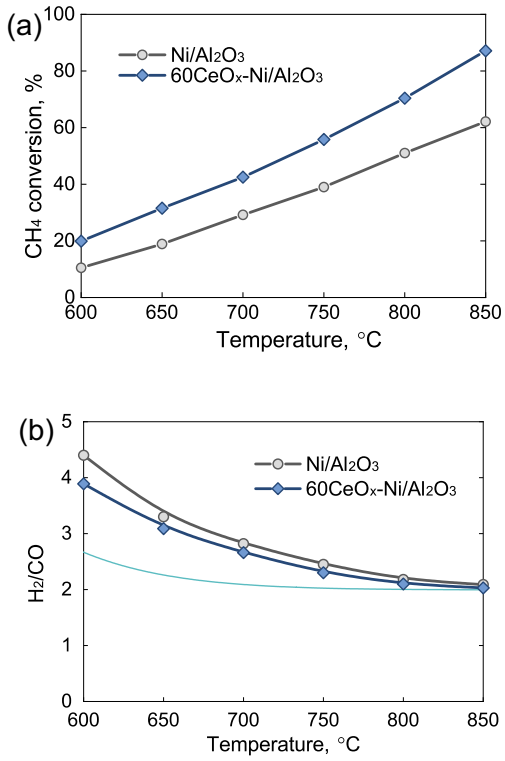

421
422

423 Figure 7. (a) CH_4 conversion and (b) H_2/CO ratio of BRM as a function of reaction temperature
424 using Ni/Al_2O_3 and $60CeO_x$-Ni/Al_2O_3. Reaction conditions: 50 mg catalyst, 30 mL/min CH_4, 10
425 mL/min CO_2, and 20 mL/min H_2O (gas phase).

426

427 Figure 8 shows the catalytic performance of uncoated Ni/Al_2O_3 and $60CeO_x$-Ni/Al_2O_3 at 750 ºC
428 and 850 ºC with different ratios of $H_2O/CO_2/CH_4$ but $(H_2O+CO_2)/CH_4=1$ in the feed as the
429 combination of DRM and SRM. In Figure 8a, the CeO_x ALD overcoating significantly enhanced
430 the CH_4 conversion for $60CeO_x$-Ni/Al_2O_3, as compared to the uncoated Ni/Al_2O_3 under different
431 feed conditions. For instance, the CH_4 conversion was 62.6% for Ni/Al_2O_3 and 87.6% for $60CeO_x$-

Ni/Al_2O_3 with a feed of $H_2O/CO_2/CH_4$=3/0/3 (which is the case of SRM) at 850 ºC. Besides, it was noted that the H_2O/CO_2 ratio in the feed influenced the CH_4 conversion. For instance, the CH_4 conversion for $60CeO_x$-Ni/Al_2O_3 with feed $H_2O/CO_2/CH_4$=0/3/3 (which is the case of DRM) was 86.2% at 850 ºC, and a higher CH_4 conversion was achieved with a higher H_2O content ratio in the feed, reaching CH_4 conversion of 87.2% with a feed of $H_2O/CO_2/CH_4$=2/1/3, and 87.6% with a feed of $H_2O/CO_2/CH_4$=2/1/3. The higher conversion for high-content H_2O in feed is more significant for Ni/Al_2O_3, with CH_4 conversion at 750 ºC reaching CH_4 conversion of 57.7% with $H_2O/CO_2/CH_4$=0/3/3 (DRM), 62.1% at $H_2O/CO_2/CH_4$=2/1/3, and 62.6% at $H_2O/CO_2/CH_4$=3/0/3 (SRM). The influence of H_2O in the feed is more significant at lower temperatures. At 750 ºC, $60CeO_x$-Ni/Al_2O_3 had a CH_4 conversion of 47.9% for DRM and 52.1% for SRM, and Ni/Al_2O_3 had a CH_4 conversion of 32.7% for DRM and 41.1% for SRM, indicating that the effects of H_2O on CH_4 conversion were less significant for $60CeO_x$-Ni/Al_2O_3. The better performance with a higher H_2O content in the feed might be ascribed to the activation of CO_2. The H_2/CO ratio at 850 ºC for both catalysts was close to the equilibrium value, whereas the H_2/CO ratio at 750 ºC was far from the equilibrium value, especially for Ni/Al_2O_3. Similar to the previous discussion, the H_2/CO ratio might be affected by the water-gas shift reaction and the activation process for H_2O or CO_2. It seems that the CeO_x overcoating could enhance the CO_2 activation and achieve a H_2/CO ratio which was close to the equilibrium value.

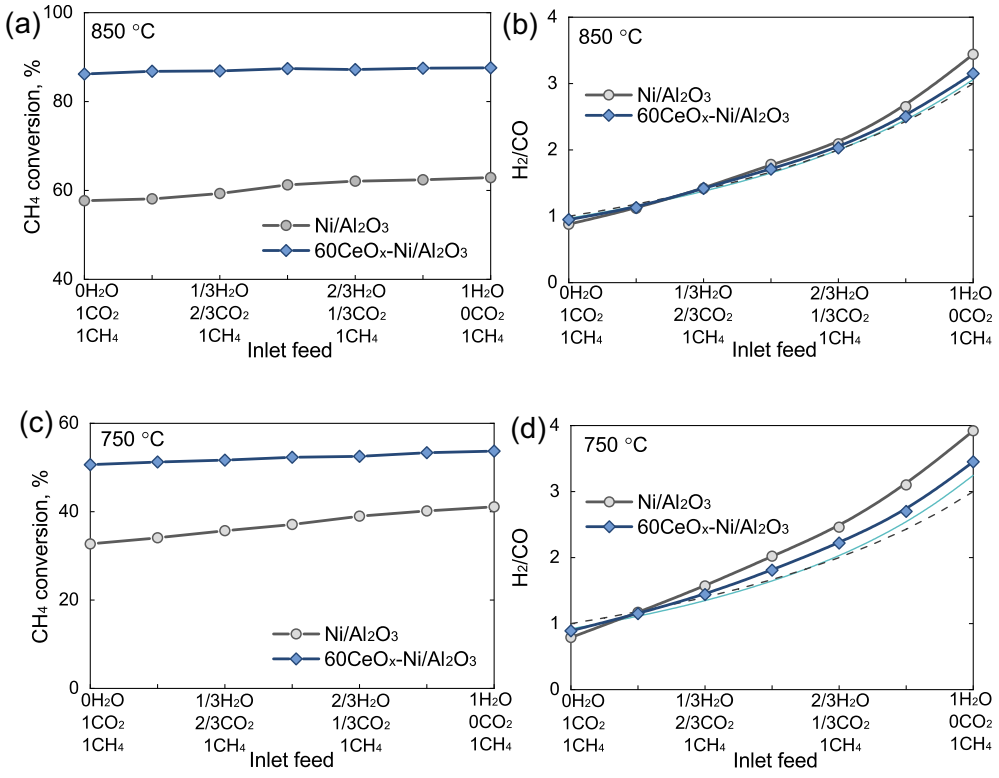

Figure 8. (a) CH_4 conversion and (b) H_2/CO ratio of BRM as a function of feed conditions using Ni/Al_2O_3 and $60CeO_x$-Ni/Al_2O_3 as catalysts at 850 ºC. (c) CH_4 conversion and (d) H_2/CO ratio of BRM as a function of feed conditions using Ni/Al_2O_3 and $60CeO_x$-Ni/Al_2O_3 as catalysts at 750 ºC. Reaction conditions: 50 mg catalyst and inlet feed $(H_2O+CO_2)/CH_4$=1.

H_2 pulse chemisorption was conducted to demonstrate the confinement effects and the promoting effects of CeO_x overcoating on Ni/Al_2O_3 for BRM reaction, as shown in Figure 9. With the increase in the cycle number of CeO_x ALD overcoating, the Ni surface area exhibited a decreasing trend, which indicates that the CeO_x overcoating partially covered the Ni surface and confined the Ni sites. The turnover frequency (TOF) was also calculated to investigate the intrinsic reaction activity with the order as follows: $90CeO_x$-Ni/Al_2O_3 ≈ $60CeO_x$-Ni/Al_2O_3 > $30CeO_x$-Ni/Al_2O_3 >

464 Ni/Al_2O_3. The increasing TOF value with the increase in the ALD cycle number indicates that the

465 CeO_x overcoating enhanced the intrinsic reaction rate.

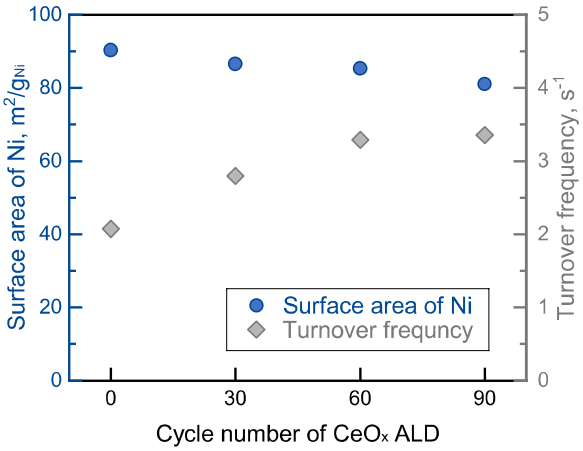

466

467 Figure 9. Ni surface area based on H_2-chemisorption and turnover frequency of methane on Ni

468 sites for bi-reforming of methane as the function of CeO_x ALD cycle number on Ni/Al_2O_3.

469

470 3.3. Characterizations of spent catalysts

471 The sintering of Ni NPs is generally one of the main reasons for catalyst deactivation. TEM was

472 used to investigate the Ni NPs size for the spent catalysts in Figure 10. For the spent Ni/Al_2O_3

473 catalyst in Figure 10a, the average size for Ni NPs was 24.6 ± 5.2 nm. For the spent $60CeO_x$-

474 Ni/Al_2O_3 catalyst in Figure 10b, the average size for Ni was 18.4 ± 3.8 nm. The presence of CeO_x

475 ALD overcoating greatly prevented the mobilization of Ni NPs, possibly due to the Ni-CeO_x

476 interaction or the geometric confinement effect of CeO_x coating [45], thus preventing the sintering

477 of Ni NPs and enhancing the stability of the Ni NPs.

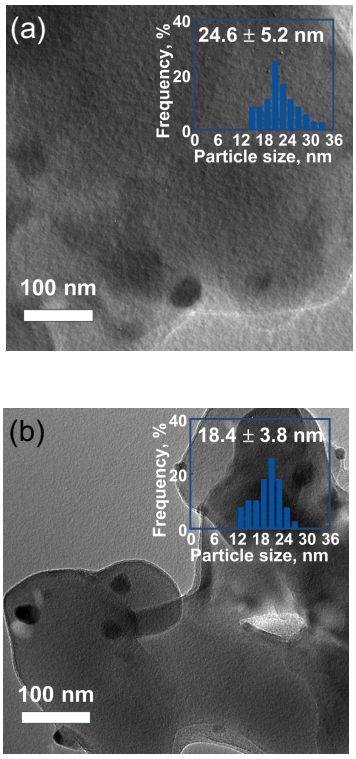

Figure 10. TEM images of (a) spent Ni/Al_2O_3 and (b) spent $60CeO_x$-Ni/Al_2O_3 after bi-reforming of methane reaction at 850 ºC for 72 h. The inset images show the size distribution of Ni NPs.

During SRM or DRM, the catalytic dissociation of methane on metal sites is generally considered as the initial step to generate H and CH_x (x=0-3) and the oxidants (H_2O or CO_2) will undergo dissociation and activation for the oxidation of CH_x. However, the side reactions (CH_4 cracking and Boudouard reaction) share the same species as carbon intermediates in the elementary step and inevitably result in carbon growth [10, 13]. During methane reforming, the carbon formation resulted from the side reactions and the low oxidation rate of coke by the reactants (i.e., H_2O and CO_2). To determine the carbon growth rate during the bi-reforming of methane, O_2-TPO was conducted on the spent catalysts. As shown in Figure 11a, spent Ni/Al_2O_3, spent $30CeO_x$-Ni/Al_2O_3, spent $60CeO_x$-Ni/Al_2O_3, and spent $90CeO_x$-Ni/Al_2O_3 after bi-reforming of methane at 850 ºC for

492 72 h ($H_2O/CO_2/CH_4$ =2/1/3) were tested. The oxidation temperature of the surface carbon on these
493 catalysts ranged from 300 to 750 ºC, indicating different carbon species. According to the
494 oxidation temperature, the chemical composition and crystallization of carbon can be determined.
495 The carbon peak at <400 ºC was assigned to the carbidic carbon (C_α), the carbon peak at 400-600
496 ºC was assigned to the amorphous carbon (C_β), and the carbon peak at > 600 ºC was assigned to
497 the graphitic carbon (C_γ) [46, 47]. In this work, all three carbon species resulted from the bi-
498 reforming of methane reaction, especially for the amorphous carbon and graphitic carbon. As for
499 the catalysts with CeO_x ALD overcoating, there exhibited a great decrease in the carbon amount,
500 mainly for the amorphous carbon and graphitic carbon. Studies showed that further graphitization
501 growth was catalyzed on the large Ni NPs and insufficient oxidation rate. The CeO_x overcoating
502 on Ni NPs by made the Ni sites discontinuously exposed, then limited the graphitization growth.
503 Besides, the oxygen sites on CeO_x, especially the oxygen vacancies, provided the activation sites
504 for CO_2 or H_2O and enabled the high concentration of surface O for carbon oxidation. Therefore,
505 a decreasing amount of carbon deposition was found with the increase in the number of CeO_x ALD
506 cycles. TGA was also conducted to determine the carbon deposition on spent Ni/Al_2O_3 and spent
507 $60CeO_x$-Ni/Al_2O_3, as shown in Figure 11b. The catalysts first underwent a preheating process at
508 200 °C to remove any moisture. When the temperature ramped from 200 to 900 °C, the weight of
509 Ni/Al_2O_3 decreased from 98.6% to 96.5%, indicating that 2.1 wt.% coke was detected. Besides,
510 the decrease at ~120 min indicates the existence of graphitic carbon. In comparison, the weight of
511 $60CeO_x$-Ni/Al_2O_3 decreased from 99.0% to 98.2%, indicating 0.8 wt.% coke was detected. The
512 lower coke amount was ascribed to the activation sites of H_2O and CO_2 on Ni-CeO_x interface.
513 Therefore, the suppressing effects of CeO_x overcoating on coking was confirmed for Ni/Al_2O_3 in
514 the methane reforming.

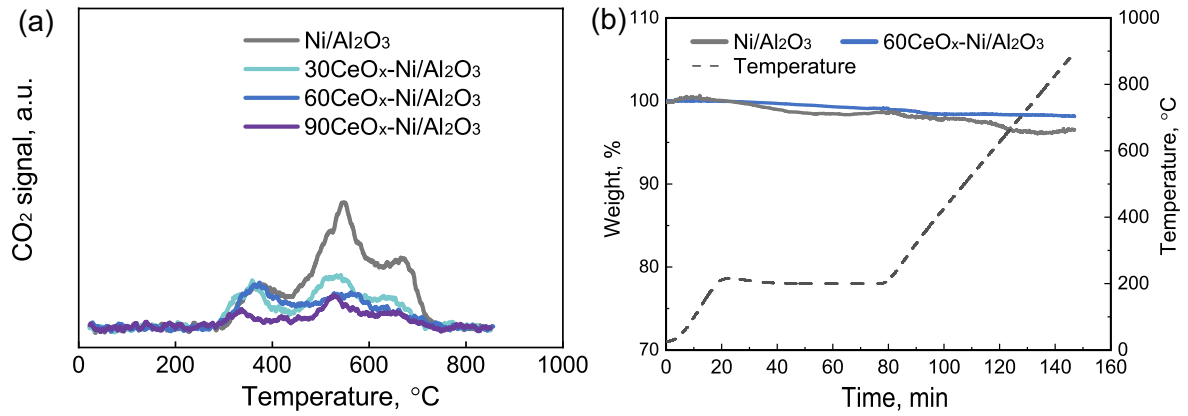

Figure 11. (a) O_2-TPO of spent Ni/Al_2O_3, $30CeO_x$-Ni/Al_2O_3, $60CeO_x$-Ni/Al_2O_3, and $90CeO_x$-Ni/Al_2O_3, (b) TGA of the spent Ni/Al_2O_3 and spent $60CeO_x$-Ni/Al_2O_3. Spent catalysts underwent bi-reforming of methane at 850 ºC for 72 h ($H_2O/CO_2/CH_4$ =2/1/3).

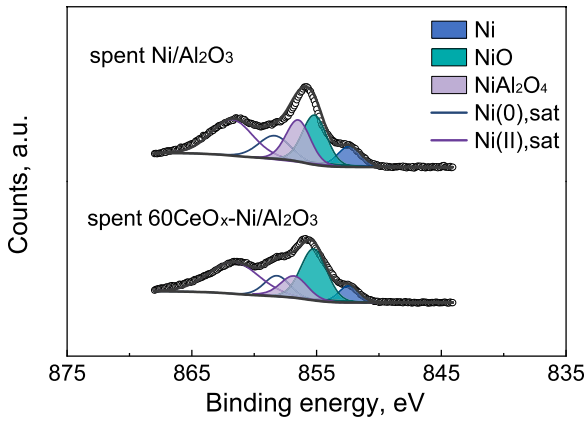

Figure 12. XPS spectra of Ni 2p3/2 of spent Ni/Al_2O_3 and spent $60CeO_x$-Ni/Al_2O_3 after bi-reforming of methane at 850 ºC for 72 h ($H_2O/CO_2/CH_4$ =2/1/3).

XPS spectra were collected using the spent Ni/Al_2O_3 and spent $60CeO_x$-Ni/Al_2O_3 catalysts after bi-reforming of methane at 850 ºC for 72 h, as shown in Figure 12 and Figure S6. For Ni 2p3/2, there was 19.9% $NiAl_2O_4$ for spent Ni/Al_2O_3 and 13.2% $NiAl_2O_4$ for spent $60CeO_x$-Ni/Al_2O_3. This indicates that the CeO_x overcoating enhanced the reducibility of $NiAl_2O_4$. Besides, it was noticed

that there was more metallic Ni for the spent $60CeO_x$-Ni/Al_2O_3 catalyst than that of spent Ni/Al_2O_3, which demonstrates that the CeO_x overcoating enhanced the reducibility and helped prevent the Ni nanoparticles from oxidation. The more metallic Ni sites by CeO_x overcoating means better utilization of Ni sites and better catalytic performance. Besides, for the O 1s spectra, the $60CeO_x$-Ni/Al_2O_3 catalyst still had a high amount of surface oxygen after the reaction process, indicating that the oxygen species of CeO_x overcoating was stable during the reaction.

3.4. Mechanism of performance enhancement by CeO_x ALD overcoating

In this work, the effects of CeO_x ALD overcoating on Ni/Al_2O_3 for bi-reforming of methane was systematically studied. The mechanism of performance enhancement was proposed, as shown in Figure S7. The CeO_x ALD overcoating was successfully deposited onto Ni/Al_2O_3 and a beneficial Ni-CeO_x interface was formed. The CeOx ALD overcoating exhibited its unique chemical properties for enhanced performance as compared to the ALD Al_2O_3 or IW CeO_2 promoter. Compared to the lower reducibility of the Al_2O_3 ALD coated Ni/Al_2O_3 catalyst due to the formation of $NiAl_2O_4$ during Al_2O_3 ALD process, the CeO_x ALD overcoating greatly improved the reducibility of Ni(II) and prevented the oxidation of the active Ni NPs. Besides, CeO_x was oxygen-deficient in non-stoichiometric form, resulting in the high concentration of the oxygen vacancies. The high oxygen vacancies in CeO_x ALD overcoating CeO_2 promoter provided higher activity in the CO_2 activation process and promoted the catalytic performance.

4. Conclusion

In this work, Ni/Al_2O_3 catalyst was prepared by depositing Ni NPs on Al_2O_3 NPs by ALD, followed by CeO_x ALD overcoating on Ni/Al_2O_3 catalyst with different numbers of cycles (i.e.,

10, 30, 60, and 90). The catalytic performance of CeO_x-Ni/Al_2O_3 was investigated for the bi-reforming of methane reaction. Based on TEM analysis, the Ni NPs size for the pristine Ni/Al_2O_3 catalyst was about 2.7 nm and the Ni size for the 60CeO_x-Ni/Al_2O_3 catalyst was about 2.9 nm, which indicates that the CeO_x ALD coating didn't change the morphology of Ni NPs due to its mild temperature ALD conditions. Based on XPS and CO_2-TPD, CeO_x ALD overcoating was found to be in non-stoichiometric form with a high amount of Ce(III) and oxygen vacancies, which might be ascribed to the unique ALD growth process. Besides, the reduction process for the catalyst led to a further reduction of Ce(IV) to Ce(III) and generated more oxygen vacancies, which acted as the CO_2 activation sites and achieved a good balance between SRM and DRM. Based on TPR analysis, CeO_x ALD also enhanced the reducibility of Ni NPs and helped keep Ni in the metallic state. For the bi-reforming of methane, CeO_x ALD significantly improved the activity and stability and achieved a better control in the H_2/CO ratio at the designed $H_2O/CO_2/CH_4$ feed. For BRM at 850 ºC with $H_2O/CO_2/CH_4$=2/1/3, which was intended to produce H_2/CO at 2, the CH_4 conversion was ~61.9% for pristine Ni/Al_2O_3 and 87.2% for 60CeO_x-Ni/Al_2O_3, with H_2/CO molar ratio at ~2.05 for both catalysts. For BRM at 750 ºC with $H_2O/CO_2/CH_4$/=2/1/3, the CH_4 conversion was ~39.4% with gradual deactivation for pristine Ni/Al_2O_3 and ~53.5% in a 150-h test for 60CeO_x-Ni/Al_2O_3. Besides, the H_2/CO varied from 2.45 to 2.88 for Ni/Al_2O_3 during a 75-h test and kept stable at 2.34 for 60CeO_x-Ni/Al_2O_3. Under the varying $H_2O/CO_2/CH_4$ feed conditions (keeping (H_2O+CO_2)/CH_4=1), the 60CeO_x-Ni/Al_2O_3 catalyst exhibited a closer H_2/CO value to the direct stoichiometric combination result of SRM and DRM than that of the Ni/Al_2O_3 catalyst. Based on TPO results of spent catalysts, CeO_x ALD significantly decreased the carbon formation, especially the amorphous carbon and graphitic carbon, because CeO_x ALD overcoating could

provide sufficient oxygen vacancies, which enhanced the oxidant activation to remove carbon intermediate and inhibited carbon formation.

Acknowledgment

This work was supported in part by the U.S. National Science Foundation (Award Number 2306177).

References

[1] Y. Song, E. Ozdemir, S. Ramesh, A. Adishev, S. Subramanian, A. Harale, M. Albuali, B.A. Fadhel, A. Jamal, D. Moon, Dry reforming of methane by stable Ni–Mo nanocatalysts on single-crystalline MgO, Science, 367 (2020) 777-781.
[2] D. Gielen, R. Gorini, N. Wagner, R. Leme, L. Gutierrez, G. Prakash, E. Asmelash, L. Janeiro, G. Gallina, G. Vale, Global energy transformation: A roadmap to 2050, (2019).
[3] G.A. Olah, A. Goeppert, M. Czaun, G.S. Prakash, Bi-reforming of methane from any source with steam and carbon dioxide exclusively to metgas ($CO–2H_2$) for methanol and hydrocarbon synthesis, Journal of the American Chemical Society, 135 (2013) 648-650.
[4] G.A. Olah, A. Goeppert, M. Czaun, T. Mathew, R.B. May, G.S. Prakash, Single step bi-reforming and oxidative bi-reforming of methane (natural gas) with steam and carbon dioxide to metgas ($CO-2H_2$) for methanol synthesis: Self-sufficient effective and exclusive oxygenation of methane to methanol with oxygen, Journal of the American Chemical Society, 137 (2015) 8720-8729.
[5] A. Saravanan, D.-V.N. Vo, S. Jeevanantham, V. Bhuvaneswari, V.A. Narayanan, P. Yaashikaa, S. Swetha, B. Reshma, A comprehensive review on different approaches for CO_2 utilization and conversion pathways, Chemical Engineering Science, (2021) 116515.
[6] X. Fan, B. Jin, S. Ren, S. Li, M. Yu, X. Liang, Roles of interaction between components in CZZA/HZSM-5 catalyst for dimethyl ether synthesis via CO_2 hydrogenation, AIChE Journal, 67 (2021) e17353.
[7] X. Fan, S. Ren, B. Jin, S. Li, M. Yu, X. Liang, Enhanced stability of Fe-modified CuO-ZnO-ZrO_2-Al_2O_3/HZSM-5 bifunctional catalysts for dimethyl ether synthesis from CO_2 hydrogenation, Chinese Journal Of Chemical Engineering, 38 (2021) 106-113.
[8] X. Yan, T. Hu, P. Liu, S. Li, B. Zhao, Q. Zhang, W. Jiao, S. Chen, P. Wang, J. Lu, Highly efficient and stable Ni/CeO_2-SiO_2 catalyst for dry reforming of methane: Effect of interfacial structure of Ni/CeO_2 on SiO_2, Applied Catalysis B: Environmental, 246 (2019) 221-231.
[9] Y.-x. Pan, P. Kuai, Y. Liu, Q. Ge, C.-j. Liu, Promotion effects of Ga_2O_3 on CO_2 adsorption and conversion over a SiO_2-supported Ni catalyst, Energy & Environmental Science, 3 (2010) 1322-1325.

[10] M. Akri, S. Zhao, X. Li, K. Zang, A.F. Lee, M.A. Isaacs, W. Xi, Y. Gangarajula, J. Luo, Y. Ren, Atomically dispersed nickel as coke-resistant active sites for methane dry reforming, Nature Communications, 10 (2019) 1-10.
[11] B. Qi, O. Farid, A.F. Velo, J. Mendil, S. Uribe, Y. Kaneko, K. Sakakura, Y. Kagota, M. Al-Dahhan, Tracking the heavy metal contaminants entrained with the flow into a trickle bed hydrotreating reactor packed with different catalyst shapes using newly developed noninvasive dynamic radioactive particle tracking, Chemical Engineering Journal, 429 (2022) 132277.
[12] B. Qi, S. Uribe, O. Farid, M. Al-Dahhan, Development of a hybrid pressure drop and liquid holdup phenomenological model for trickle bed reactors based on two-phase volume averaged equations, The Canadian Journal of Chemical Engineering, 99 (2021) 1811-1823.
[13] Y. Lou, M. Steib, Q. Zhang, K. Tiefenbacher, A. Horváth, A. Jentys, Y. Liu, J.A. Lercher, Design of stable Ni/ZrO_2 catalysts for dry reforming of methane, Journal of Catalysis, 356 (2017) 147-156.
[14] Y. Liu, Y. Wu, Z. Akhtamberdinova, X. Chen, G. Jiang, D. Liu, Dry reforming of shale gas and carbon dioxide with Ni-Ce-Al_2O_3 catalyst: Syngas production enhanced over Ni-CeO_x formation, ChemCatChem, 10 (2018) 4689-4698.
[15] X. Du, D. Zhang, L. Shi, R. Gao, J. Zhang, Morphology dependence of catalytic properties of Ni/CeO_2 nanostructures for carbon dioxide reforming of methane, The Journal of Physical Chemistry C, 116 (2012) 10009-10016.
[16] Z. Wang, Z. Huang, J.T. Brosnahan, S. Zhang, Y. Guo, Y. Guo, L. Wang, Y. Wang, W. Zhan, Ru/CeO_2 catalyst with optimized CeO_2 support morphology and surface facets for propane combustion, Environmental Science & Technology, 53 (2019) 5349-5358.
[17] F. Jiang, S. Wang, B. Liu, J. Liu, L. Wang, Y. Xiao, Y. Xu, X. Liu, Insights into the influence of CeO_2 crystal facet on CO_2 hydrogenation to methanol over Pd/CeO_2 catalysts, ACS Catalysis, 10 (2020) 11493-11509.
[18] J. Vecchietti, A. Bonivardi, W. Xu, D. Stacchiola, J.J. Delgado, M. Calatayud, S.n.E. Collins, Understanding the role of oxygen vacancies in the water gas shift reaction on ceria-supported platinum catalysts, ACS Catalysis, 4 (2014) 2088-2096.
[19] I. Luisetto, S. Tuti, C. Romano, M. Boaro, E. Di Bartolomeo, J.K. Kesavan, S.S. Kumar, K. Selvakumar, Dry reforming of methane over Ni supported on doped CeO_2: New insight on the role of dopants for CO_2 activation, Journal of CO_2 Utilization, 30 (2019) 63-78.
[20] L. Cao, J. Lu, Atomic-scale engineering of metal–oxide interfaces for advanced catalysis using atomic layer deposition, Catalysis Science & Technology, 10 (2020) 2695-2710.
[21] L. Cao, W. Liu, Q. Luo, R. Yin, B. Wang, J. Weissenrieder, M. Soldemo, H. Yan, Y. Lin, Z. Sun, Atomically dispersed iron hydroxide anchored on Pt for preferential oxidation of CO in H_2, Nature, 565 (2019) 631-635.
[22] X. Wang, B. Jin, Y. Jin, T. Wu, L. Ma, X. Liang, Supported single Fe atoms prepared via atomic layer deposition for catalytic reactions, ACS Applied Nano Materials, 3 (2020) 2867-2874.
[23] X. Wang, C. Zhang, B. Jin, X. Liang, Q. Wang, Z. Zhao, Q. Li, Pt–Carbon interaction-determined reaction pathway and selectivity for hydrogenation of 5-hydroxymethylfurfural over carbon supported Pt catalysts, Catalysis Science & Technology, 11 (2021) 1298-1310.
[24] H. Yan, K. He, I.A. Samek, D. Jing, M.G. Nanda, P.C. Stair, J.M. Notestein, Tandem In_2O_3-Pt/Al_2O_3 catalyst for coupling of propane dehydrogenation to selective H_2 combustion, Science, 371 (2021) 1257-1260.

[25] J. Lu, B. Fu, M.C. Kung, G. Xiao, J.W. Elam, H.H. Kung, P.C. Stair, Coking-and sintering-resistant palladium catalysts achieved through atomic layer deposition, Science, 335 (2012) 1205-1208.
[26] Z. Shang, X. Liang, "Core–shell" nanostructured supported size-selective catalysts with high catalytic activity, Nano letters, 17 (2017) 104-109.
[27] Z. Lu, R.W. Tracy, M.L. Abrams, N.L. Nicholls, P.T. Barger, T. Li, P.C. Stair, A.A. Dameron, C.P. Nicholas, C.L. Marshall, Atomic layer deposition overcoating improves catalyst selectivity and longevity in propane dehydrogenation, ACS Catalysis, 10 (2020) 13957-13967.
[28] T.M. Onn, S. Zhang, L. Arroyo-Ramirez, Y.-C. Chung, G.W. Graham, X. Pan, R.J. Gorte, Improved thermal stability and methane-oxidation activity of Pd/Al_2O_3 catalysts by atomic layer deposition of ZrO_2, ACS Catalysis, 5 (2015) 5696-5701.
[29] B. Jin, S. Li, Y. Liu, X. Liang, Engineering metal-oxide interface by depositing ZrO_2 overcoating on Ni/Al_2O_3 for dry reforming of methane, Chemical Engineering Journal, 436 (2022) 135195.
[30] K. Yuan, Q. Cao, H.-L. Lu, M. Zhong, X. Zheng, H.-Y. Chen, T. Wang, J.-J. Delaunay, W. Luo, L. Zhang, Oxygen-deficient WO_{3-x}@ TiO_{2-x} core–shell nanosheets for efficient photoelectrochemical oxidation of neutral water solutions, Journal of Materials Chemistry A, 5 (2017) 14697-14706.
[31] X. Liang, L.F. Hakim, G.D. Zhan, J.A. McCormick, S.M. George, A.W. Weimer, J.A. Spencer, K.J. Buechler, J. Blackson, C.J. Wood, Novel processing to produce polymer/ceramic nanocomposites by atomic layer deposition, Journal of the American Ceramic Society, 90 (2007) 57-63.
[32] G. Pantaleo, V. La Parola, F. Deganello, R. Singha, R. Bal, A. Venezia, Ni/CeO_2 catalysts for methane partial oxidation: Synthesis driven structural and catalytic effects, Applied Catalysis B: Environmental, 189 (2016) 233-241.
[33] R.-P. Ye, Q. Li, W. Gong, T. Wang, J.J. Razink, L. Lin, Y.-Y. Qin, Z. Zhou, H. Adidharma, J. Tang, High-performance of nanostructured Ni/CeO_2 catalyst on CO_2 methanation, Applied Catalysis B: Environmental, 268 (2020) 118474.
[34] A. Gupta, T.S. Sakthivel, C.J. Neal, S. Koul, S. Singh, A. Kushima, S. Seal, Antioxidant properties of ALD grown nanoceria films with tunable valency, Biomaterials Science, 7 (2019) 3051-3061.
[35] J. Liu, L.R. Redfern, Y. Liao, T. Islamoglu, A. Atilgan, O.K. Farha, J.T. Hupp, Metal–organic-framework-supported and-isolated ceria clusters with mixed oxidation states, ACS Applied Materials & Interfaces, 11 (2019) 47822-47829.
[36] J.W. Shin, S. Oh, S. Lee, D. Go, J. Park, H.J. Kim, B.C. Yang, G.Y. Cho, J. An, ALD CeO_2-Coated Pt anode for thin-film solid oxide fuel cells, International Journal of Hydrogen Energy, 46 (2021) 20087-20092.
[37] M. Zhang, J. Zhang, Y. Wu, J. Pan, Q. Zhang, Y. Tan, Y. Han, Insight into the effects of the oxygen species over Ni/ZrO_2 catalyst surface on methane reforming with carbon dioxide, Applied Catalysis B: Environmental, 244 (2019) 427-437.
[38] B. Jin, S. Li, X. Liang, Enhanced activity and stability of MgO-promoted Ni/Al_2O_3 catalyst for dry reforming of methane: Role of MgO, Fuel, 284 (2021) 119082.
[39] R. Yang, C. Xing, C. Lv, L. Shi, N. Tsubaki, Promotional effect of La_2O_3 and CeO_2 on Ni/γ-Al_2O_3 catalysts for CO_2 reforming of CH_4, Applied Catalysis A: General, 385 (2010) 92-100.

[40] B. Jin, Z. Shang, S. Li, Y.-B. Jiang, X. Gu, X. Liang, Reforming of methane with carbon dioxide over cerium oxide promoted nickel nanoparticles deposited on 4-channel hollow fibers by atomic layer deposition, Catalysis Science & Technology, 10 (2020) 3212-3222.
[41] A. Ruiz Puigdollers, P. Schlexer, S. Tosoni, G. Pacchioni, Increasing oxide reducibility: The role of metal/oxide interfaces in the formation of oxygen vacancies, ACS Catalysis, 7 (2017) 6493-6513.
[42] J.L. Ewbank, L. Kovarik, F.Z. Diallo, C. Sievers, Effect of metal–support interactions in Ni/Al_2O_3 catalysts with low metal loading for methane dry reforming, Applied Catalysis A: General, 494 (2015) 57-67.
[43] X. Jia, X. Zhang, N. Rui, X. Hu, C.-j. Liu, Structural effect of Ni/ZrO_2 catalyst on CO_2 methanation with enhanced activity, Applied Catalysis B: Environmental, 244 (2019) 159-169.
[44] B. Jin, S. Li, X. Liang, High-performance catalytic four-channel hollow fibers with highly dispersed nickel nanoparticles prepared by atomic layer deposition for dry reforming of methane, Industrial & Engineering Chemistry Research, (2021).
[45] Y. Zhang, A. Chen, M.-W. Kim, A. Alaei, S.S. Lee, Nanoconfining solution-processed organic semiconductors for emerging optoelectronics, Chemical Society Reviews, 50 (2021) 9375-9390.
[46] L. Li, S. He, Y. Song, J. Zhao, W. Ji, C.-T. Au, Fine-tunable Ni@ porous silica core–shell nanocatalysts: Synthesis, characterization, and catalytic properties in partial oxidation of methane to syngas, Journal of Catalysis, 288 (2012) 54-64.
[47] L. Chen, Y. Lu, Q. Hong, J. Lin, F. Dautzenberg, Catalytic partial oxidation of methane to syngas over Ca-decorated-Al_2O_3-supported Ni and NiB catalysts, Applied Catalysis A: General, 292 (2005) 295-304.